Steel and Composite Structures, *Vol. 22, No. 2 (2016) 217-234*
DOI: http://dx.doi.org/10.12989/scs.2016.22.2.217

Studies on T-Shaped composite columns consist of multi separate concrete-filled square tubular steel sections under eccentric axial load

Bin Rong [1,2a], Guangchao You [1b], Ruoyu Zhang [*1], Changxi Feng [1] and Rui Liu [1]

[1] *Department of Civil Engineering, Tianjin University, Tianjin, 300072, China*
[2] *Key Laboratory of Coast Civil Structure Safety, Tianjin University, Tianjin, 300072, China*

(*Received June 12, 2016, Revised September 17, 2016, Accepted September 29, 2016*)

Abstract. In order to investigate mechanical properties and load-bearing capacity of T-shaped Concrete-Filled Square Steel Tubular (TCFST) composite columns under eccentric axial load, three T-shaped composite columns were tested under eccentric compression. Experimental results show that failure mode of the columns under eccentric compression was bending buckling of the whole specimen, and mono column performs flexural buckling. Specimens behaved good ductility and load-bearing capacity. Nonlinear finite element analysis was also employed in this investigation. The failure mode, the load-displacement curve and the ultimate bearing capacity of the finite element analysis are in good agreement with the experimental ones. Based on eccentric compression test and parametric finite element analysis, the calculation formula for the equivalent slenderness ratio was proposed and the bearing capacity of TCFST composite columns under eccentric compression was calculated. Results of theoretical calculation, parametric finite element analysis and eccentric compression experiment accord well with each other, which indicates that the theoretical calculation method of the bearing capacity is advisable.

Keywords: TCFST; finite element analysis; bearing capacity; the equivalent slenderness ratio; eccentric compression test

1. Introduction

Concrete-filled square steel tubular composite column is composed of four concrete-filled square steel tubular columns connected by perforated connecting plates. Compared to regular columns, each mono column of the concrete-filled square steel tubular composite column has a smaller section and they can be embodied in walls, as shown in Fig. 1. It not only makes full use of the high bearing capacity of concrete-filled square steel tubular columns connected, mechanical properties such as good plasticity and toughness, but also has the advantages of flexible arrangement, graceful architectural form and increases the usable area of the building. Concrete-filled square steel tubular composite column has been applied to the post-disaster reconstruction of WenChuan earthquake and other projects. In the past, the special-shaped column has been widely

*Corresponding author, Ph.D., E-mail: zryu@163.com
[a] Ph.D., E-mail: tjerobin@126.com
[b] Ph.D. Student, E-mail: youguangchao@163.com

http://www.techno-press.org/?journal=scs&subpage=6 ISSN: 1229-9367 (Print), 1598-6233 (Online)

studied. The results of experimental investigation, numerical calculation and theoretical analysis on axial compression ratio limit values for steel reinforced concrete (SRC) special shaped columns were presented (Chen *et al*. 2016). The behavior of axially loaded concrete-filled steel tubular stub columns with special-shaped cross-sections (Ren *et al*. 2014) and T-shaped (Tu *et al*. 2014) were studied. Nine T-shaped Steel Reinforced Concrete Special Shaped (SRCSS) columns, four L-shaped SRCSS columns and four X-shaped SRCSS columns were tested to examine the effects of shape steel configuration, loading angle, axial compressive ratio and shear-span ratio on the behavior (strength, stiffness, energy dissipation, ductility, etc.) of SRCSS column specimens by Chen *et al*. (2015). An experimental research was conducted to investigate the strength of biaxial loaded short and slender reinforced concrete columns with high strength concrete by Dundar and Tokgoz (2008, 2012). Yang *et al*. (2010) conducted an experimental study of welding battlement-shaped bar stiffeners and tensile bar stiffeners on tube surfaces to improve the axial compressive behaviors of T-shaped CFST columns. Six specimens subjected to a constant axial load and cyclically varying lateral loading were tested to study the seismic behavior of concrete-filled L-shaped steel tube columns by Shen *et al.* (2013). The axial compression experiment and nonlinear finite element analysis were carried out to study the mechanical property of the L-shaped concrete-filled square steel tubular special-shaped column by Rong *et al*. (2012). A special-shaped column composed of concrete-filled steel tubes (SCFST column) is experimentally investigated by Zhou *et al*. (2015). Axial compression test and finite element simulation analysis of 6 concrete-filled square steel tubular special-shaped columns were conducted by Chen *et al.* (2009), and they proposed the calculation formula for axial load-bearing capacity of Concrete-filled square steel tubular special-shaped column. Zhou *et al.* (2012) researched seismic performance of concrete-filled square steel tubular special-shaped column under low reversed cyclic load. These results showed that the overall work performance and seismic performance are desirable of TCFST columns are desirable.

At present, the researches on concrete-filled square steel tubular special-shaped column are mainly focused on the axial compression and seismic performance. The researches for the compression-bending performance are short. However, actually the pillars are in the compression-bending state. Therefore, it is necessary to research on the compression-bending performance of concrete-filled square steel tubular special-shaped column. This paper will focus on investigating mechanical properties under eccentric compression and load-bearing capacity of TCFST composite columns by compression-bending test, finite element analysis and theoretical calculations.

TCFST composite column is singly symmetric section, Therefore, when determining the bending test programs, it is necessary to consider that it is one-way or two-way bending, and the position of the action point is based on the assumption of the actual design. However, in the

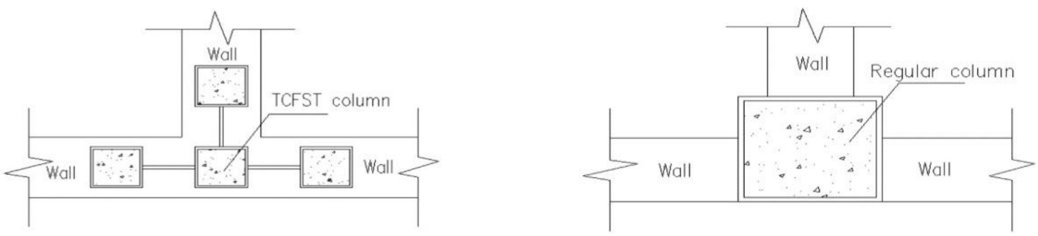

Fig. 1 Applications of a regular column and an TCFST column

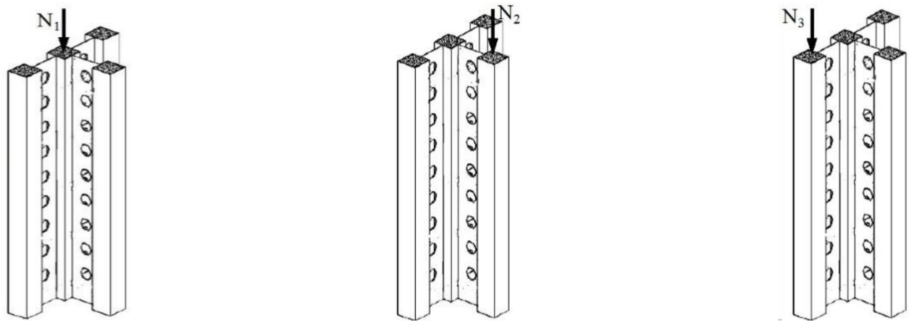

(a) GZ1 (b) GZ2 (c) GZ3

Fig. 2 Pressure on mono column of TCFST composite columns

practical engineering, when each mono column of lattice column is subjected to axial force, the difference between the axial force of the mono columns is inevitable. Once a mono column suffers a bigger axial force than others, the column is equivalent to suffer the effect of eccentric pressure. There are columns in the compression-bending state, as shown in Fig. 2.

2. Compression-bending test

2.1 Specimen design and production

The design of the specimens is based on the general residential (story height 3000 mm, wall thickness 200 mm). The scale of the specimens respect to real composite column is 0.5. There are three specimens named GZ1, GZ2 and GZ3 in the experiments, and the detailed dimensions are

Table 1 Dimensions of specimens

Column	Steel tube	Connecting plate	
$H(mm)$	$D \times D \times t_c(mm)$	$B \times t_d(mm)$	$d(mm)$
1600	$80 \times 80 \times 4$	80×6	40

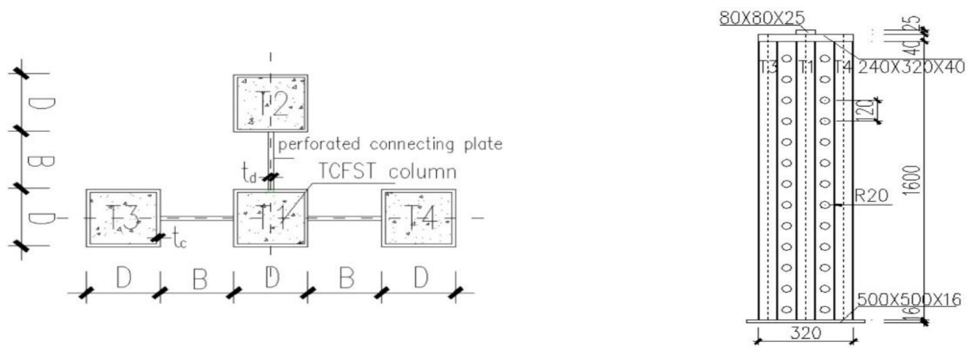

Fig. 3 Configuration of specimen

listed in Table.1 and shown in Fig. 3. They have used four separate concrete filled square tubular steel column sections (80 mm × 1600 mm × 6 mm) connected by perforated connecting plates(80mm × 1600mm × 6mm) and welded them with a base plate (500 mm × 500 mm × 16 mm) at the bottom and also welded the multi-separate steel section at the top with a plate (240 mm × 320 mm × 40 mm) (Yang and Han 2011) after the in-filled concrete was cured for two weeks. At the top one of the square sections was left out of this coverage. Then additional (80 mm × 80 mm × 25 mm) plate was welded on the top of the specimen (i.e., mono columns T1, T2 and T4). The loads are applied to the composite column through these plates.

2.2 Material properties

Standard tension coupons (200 mm × 20 mm) were cut from specimens and the concrete cubes (150 mm × 150 mm × 150 mm) were cast and cured for 28 days in the same conditions. Mechanical properties of steel and concrete were measured basing on standard test method. The yield strength f_y, the ultimate strength f_u and the steel elasticity modulus E_s are listed in Table 2, The concrete cube strength f_c and the concrete elastic modulus E_c are listed in Table 3.

2.3 Loading scheme

A 500 t capacity hydraulic testing machine was used to compress the specimens. Test setup is shown in Fig. 4. Monotonic loading method was adopted in the experiment. Loading scheme was controlled by load in the elastic range, and each load increment was 1/10 of the estimated ultimate load. Each load interval was maintained for about 3~5 minutes. Once the steel tube yield, loading scheme would be controlled by displacement, and the displacement speed was 0.3 mm/min. At the

Table 2 The mechanics performance of steel

Material	f_y (N/mm^2)	f_u (N/mm^2)	E_s (10^{5}N/mm^2)
Steel	379.1	467.9	2.115

Table 3 The mechanics performance of concrete

Material	f_{cu} (N/mm^2)	E_c (10^{4}N/mm^2)
Concrete	38.1	3.11

Fig. 4 Test setup

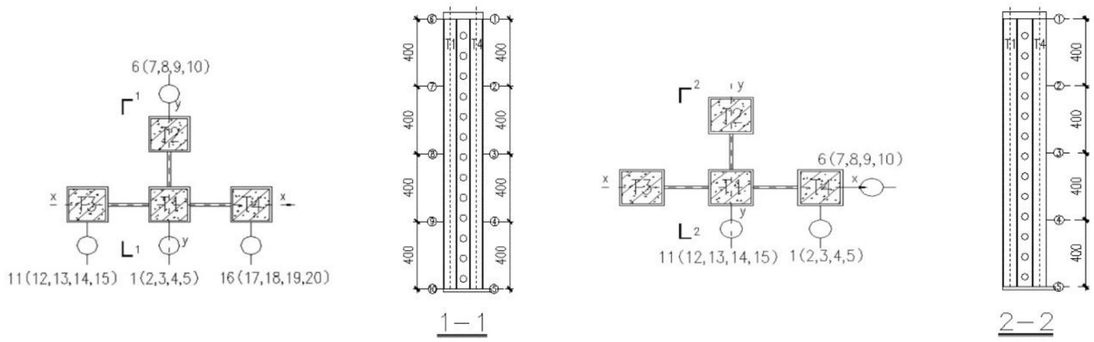

(a) GZ1 and GZ2 (b) GZ3

Fig. 5 Layout of dial indicators

same time, the corresponding deformation values of each level load were recorded continuously until the specimens failed.

2.4 Measuring-point arrangement

The main measurements were specimens bearing capacity, longitudinal displacement and deflection. Fig. 5 shows the layout of dial indicators. Twenty dial indicators were evenly arranged in each mono column of the specimen GZ1 and GZ2 along the column height. The specimen GZ3 is biaxial bending, so mono column T4 deflection of the specimen GZ3 was recorded by ten dial indicators arranged in tow way along the column height. In addition, the other five dial indicators were installed at mono column T1 along the column height. The compressive load and the vertical displacement were obtained from the force transducer and the displacement transducer inside the machine, respectively.

2.5 Test result

2.5.1 Experimental phenomena

Specimens failure models were shown in Fig. 6. For the TCFST composite columns under eccentric pressure, there was no obvious change in the appearance of the specimens. The deflection of the mono columns was very small and the deflection was almost proportional to the load from the initial stage of loading to 60% of ultimate load. When the load reached about 75% of ultimate load, the deflection of the upper 1/3 mono columns began to increase significantly. Near the ultimate load, the deformation of the component was obvious and the loading mono columns showed bending failure. During the loading process, the specimens showed good cooperative working behavior and there is no weld cracking. In the loading process, each loading mono column deformed slowly. Among them, specimen GZ1 and specimen GZ2 were one-way bending, and the failure modes were integral bending failure. Specimen GZ3 was two-way bending, and the failure modes was local failure.

2.5.2 Load-displacement curve

In the compression-bending test of TCFST composite columns, the vertical displacement increased continuously with the increase of load. Fig. 7 shows the load-displacement curve of the

(a) GZ1

(b) GZ2

(c) GZ3

Fig. 6 Failure modes

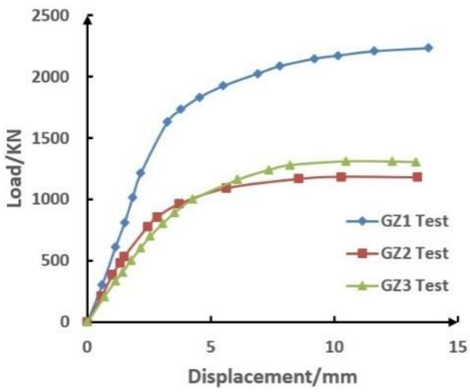

Fig. 7 Load-displacement curves

Table 4 Bearing capacity of specimens

Specimens	p_y^e (kN)	p_u^e (kN)	Δ (mm)
GZ1	1895	2233	15
GZ2	1027	1211	11
GZ3	1123	1301	12.4

specimens under eccentric pressure. All curves exhibit approximate linear rising section at the initial stage followed by an approximate horizontal section when the load is further increased. It is found that the specimens underwent obvious elastic stage and plastic stage. During the plastic stage, the bearing capacity of all specimens did not decrease with increasing displacement. It indicates that the specimens have a good ductility. The bearing capacity and stiffness of GZ1 are significantly higher than GZ2 and GZ3, because the eccentricity of GZ1 is less than GZ2 and GZ3. It shows that the eccentricity has a great influence on the bearing capacity of the specimens. The yield load P_y^e and the failure load P_u^e are obtained from the load-displacement curve of each specimen are listed in Table 4. Δ is vertical displacement corresponding to the ultimate bearing capacity.

2.5.3 Load-deflection curve

According to the test data of the dial indicators, mono columns deflection curves of TCFST composite columns at all loading levels were drawn in Figs. 8-10 (Zuo *et al*. 2012). All the deflections had a liner increment at the initial loading stage. Subsequently, there is a nonlinear deformation and the deflection increase more and more obviously. When the specimens failed, there was a large displacement in the bending way. It can be concluded that the specimens have a

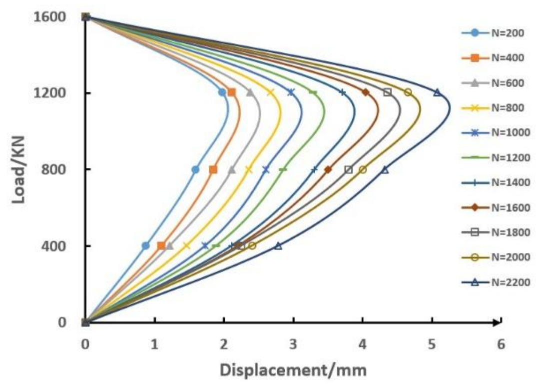

(a) Dial indicators 6, 7, 8, 9, 10 (T1)

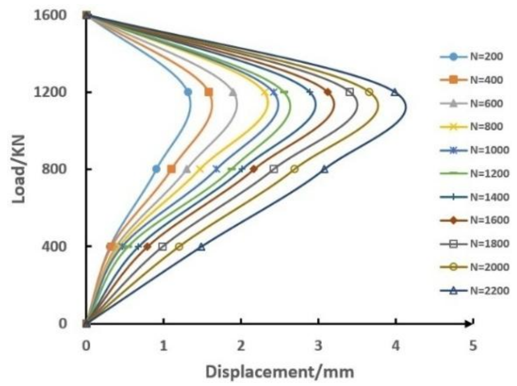

(b) Dial indicators 1, 2, 3, 4, 5 (T2)

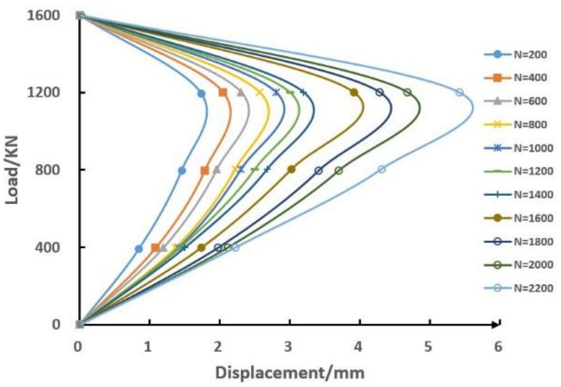

(c) Dial indicators 11, 12, 13, 14, 15 (T3)

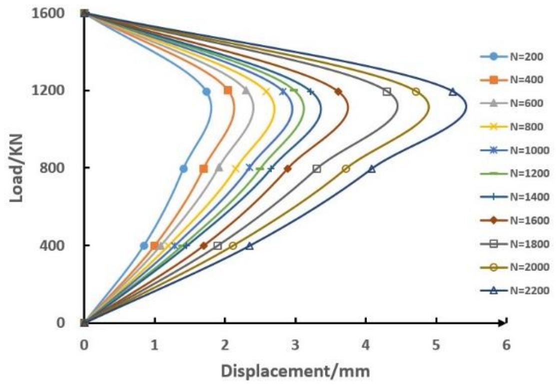

(d) Dial indicators 16, 17, 18, 19, 20 (T4)

Fig. 8 Load-deflection curves of GZ1

good ductility. Besides, the deflections of all loading mono columns are larger than others, which indicates that all the failure of all specimens was mainly caused by the destruction of the loading mono columns.

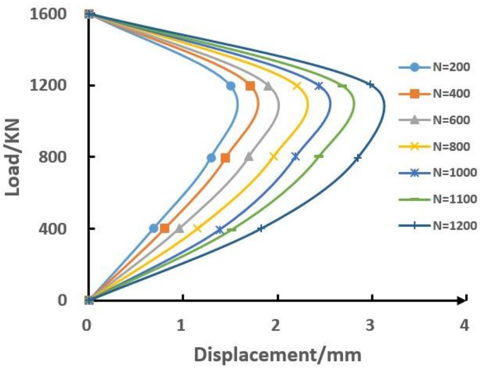

(a) Dial indicators 6, 7, 8, 9, 10 (T1)

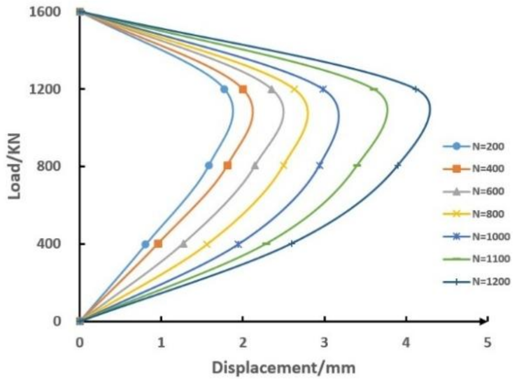

(b) Dial indicators 1, 2, 3, 4, 5 (T2)

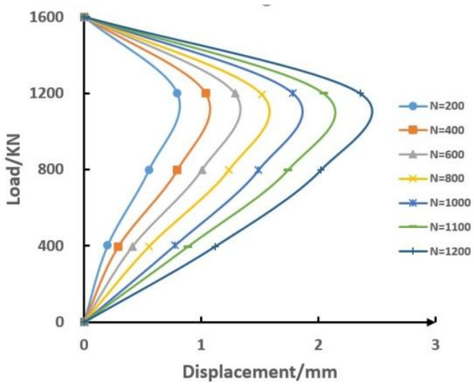

(c) Dial indicators 11, 12, 13, 14, 15 (T3)

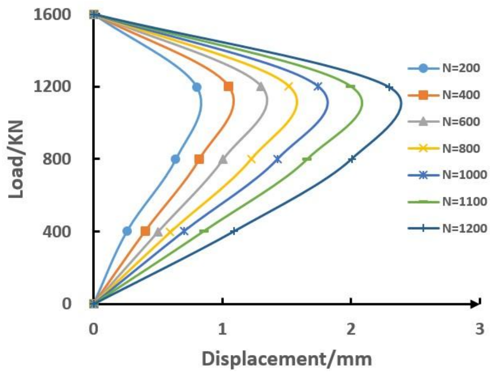

(d) Dial indicators 16, 17, 18, 19, 20 (T4)

Fig. 9 Load-deflection curves of GZ2

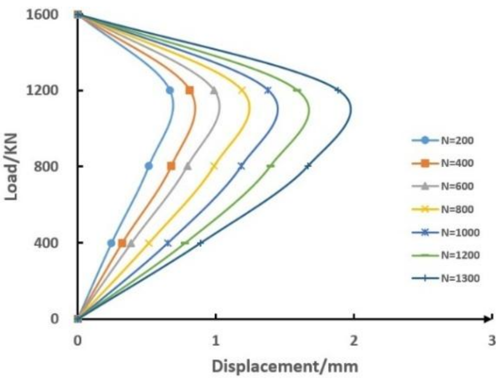

(a) Dial indicators 11, 12, 13, 14, 15 (T1)

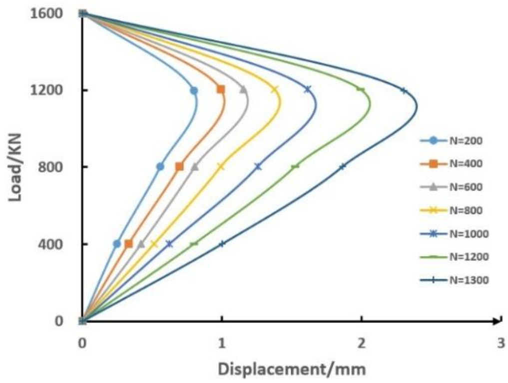

(b) Dial indicators 6, 7, 8, 9, 10 (T4-X)

Fig. 10 Load-deflection curves of GZ3

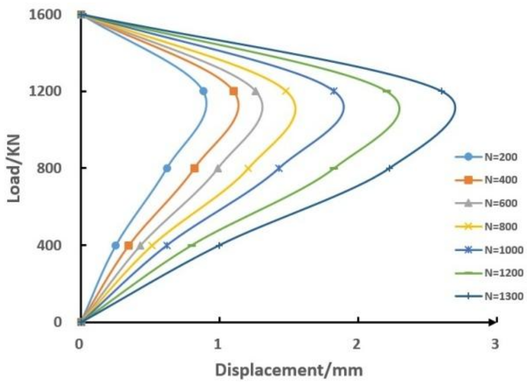

(c) Dial indicators 1, 2, 3, 4, 5 (T4-Y)

Fig. 10 Continued

3. Finite element analysis

In order to analyze failure modes and load-transferring mechanism of the mono columns and the connecting plates, a nonlinear finite element analysis has been undertaken using the finite element package ANSYS. Finite element simulation analysis of TCFST composite columns were conducted to explore the eccentric compression bearing capacity and failure form.

3.1 Finite element model

3.1.1 Modeling of the steel tubes and connecting plate

The three-dimensional 4-node element SHELL 181 was adopted to model the steel tube and the connecting plate. Each node of the element has six degrees of freedom: translations in the *x*, *y*, and *z* directions, and rotations about the *x*, *y*, and *z*-axes. This element's capacity for transverse shear deformation provides adequate accuracy in simulating the buckling behavior of the steel tubes.

As shown in Fig. 11, the constitutive law of steel tubes and connecting plates was assumed to be elastoplastic with yielding strain $\varepsilon_y = f_y/E_s$. The stress-strain relation consists of rising section and horizontal section. The strain hardening was ignored and the Poisson's ratio was equal to 0.3.

3.1.2 Concrete modeling

The three-dimensional 8-node element SOLID 65 is used to model the in-filled concrete. Each node of the element has three translation degrees of freedom in the nodal *x*, *y*, and *z* directions. This element can achieve accurate results in simulating the behavior of concrete under axial loads.

The constitutive law of concrete is used for the in-filled concrete as shown in Fig. 12. It consists of ascending and descending section. The ascending branch was assumed to be parabolic section and the descending branch was linear. The Poisson's ratio of the in-filled concrete is assumed to be 0.2, and $\varepsilon_{c0} = 1.8\sigma_{c0}/E_c$, $\varepsilon_{cu} = 0.0038$. Where, σ_{c0} and E_c are axial compressive strength of concrete and module of elasticity of concrete respectively.

3.1.3 Modeling of the concrete-steel interface

The contact elements TARGE 170 and CONTA 173 are employed to model the contact action

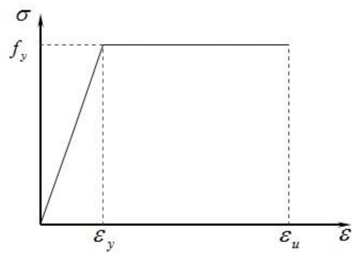

Fig. 11 Constitutive law of the steel tube and connecting plate

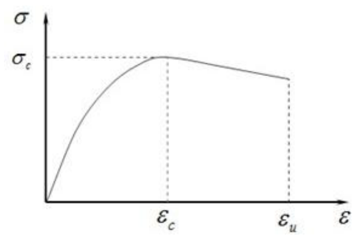

Fig. 12 Constitutive law of concrete

Fig. 13 Finite element specimen

between the steel tube and the concrete. Concrete wall is "target surface" and steel tube wall is "contact surface". TARGE170 and CONTA173 elements simulate the contact action between steel tube wall and concrete through surface-to-surface contact pairs. The friction between two faces is maintained as long as the surfaces remain in contact. The coefficient of friction between the two faces is taken as 0.25 in the analysis.

3.1.4 Modeling of loading and boundary conditions

Pinned boundary conditions were applied to the bottom surfaces of the model and all translational degrees of freedom were restrained. The static loads controlled by displacement are applied at each node of the loading surfaces, and the displacement increments are identical to the increment of test loading scheme.

3.2 The results of finite element analysis

3.2.1 Load-displacement curves

The load-displacement curves obtained from the finite element analysis are compared with the test curves in Fig. 14. The predicted load-displacement curves of all specimen have a linear elastic

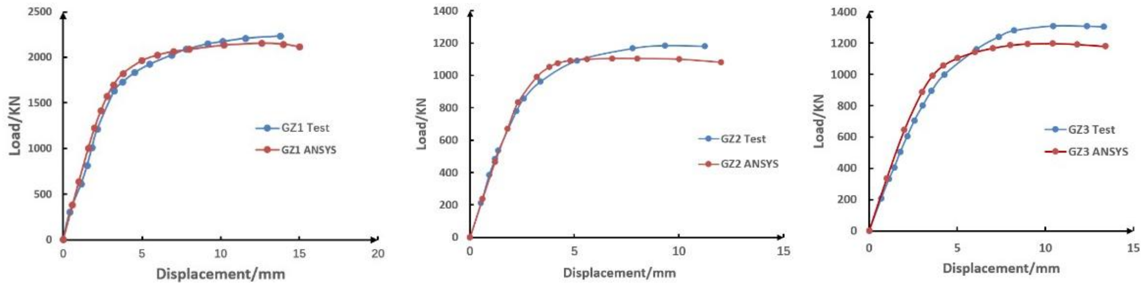

(a) GZ1 (b) GZ2 (c) GZ3

Fig. 14 Comparison of load-displacement curves

Table 5 Comparison of bearing capacity

Specimens	Ultimate bearing capacity		
	p_u^f(kN)	p_u^e(kN)	p_u^f/p_u^e
GZ1	2165	2233	0.970
GZ2	1152	1211	0.951
GZ3	1230	1301	0.945

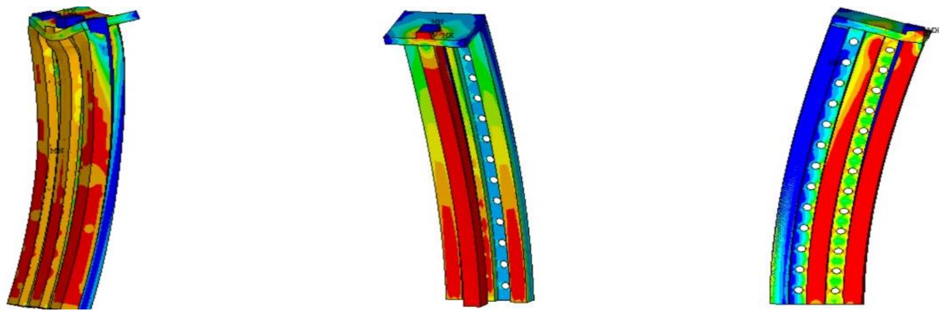

(a) GZ1 (b) GZ2 (c) GZ3

Fig. 15 Failure modes and stress contours of specimens

behavior at the initial stage followed by inelastic behavior when the load is further increased. All load-displacement curves are in good agreement with the experimental ones.

The finite element failure load p_u^f obtained from the load-displacement curves are listed in Table 5 and they are compared with the experimental ones p_u^e. From Table 5, it can be seen that the error of the ultimate bearing capacity between the finite element and the test result ranges from 3% to 6%. It can be concluded that it is feasible to analyze failure modes and load-transferring mechanism of mono columns and connect plates for finite element analysis result.

3.2.2 Failure modes and load-transferring mechanism

All specimens stress contours were obtained by finite element analysis as shown in Fig. 15. It can be seen that specimen GZ1 and GZ2 showed overall unidirectional bending failure and the vertical deformation of mono columns T1 and T2 under the pressure are larger than others. Steel and in-filled concrete of specimen GZ1 and GZ2 have reached the ultimate stress and failure occurred. Specimen GZ3 is overall bidirectional bending failure. There are significant vertical deformation and bending deflection in the mono columns T3. It can be found that the damage area of all specimens is mainly concentrated in the vicinity of loading mono columns. The connecting plates have obvious stress concentration around the opening. It can be concluded that the specimens would fail when the loading mono column reached their ultimate strength, which agrees well with the test result.

4. Theoretical calculation

The overall agreement between the experimental and the numerical results demonstrates the feasibility and accuracy of the finite element analysis. According to results of experiments and finite element analysis, an analytical method for calculation of bearing capacity of these specimens is studied based on the yielding criterion of the cross-sectional edge stresses.

4.1 Compression-bending capacity

Concrete-filled square steel tubular composite column is composed of four Concrete-Filled square steel Tubular columns connected by perforated connecting plates. As Concrete-filled square steel tubular lattice column, the calculation formula of bending bearing capacity derived from the edge yield criteria (Leonard and George 2005) can be expressed as

$$\frac{N - A_c f_c}{A_s} + \frac{M_x}{W_{1x}\left(1 - \varphi_x \frac{N}{N'_{Ex}}\right)} + \frac{M_y}{W_{1y}} \leq f \tag{1}$$

Where, $N'_{Ex} = \frac{N_{Ex}}{\gamma_R} = \frac{\pi^2 EA}{1.1\lambda_{0x}^2}$, M_x is the maximum moment against X axis, M_y is the maximum moment against Y axis, W_{1x} and W_{1y} is the gross section modulus against X axis and Y axis of the flange under larger pressure, φ_x is stability coefficient of axial compression.

4.2 Calculation for the equivalent slenderness ratio

In the bending bearing capacity formula, N'_{Ex} and φ_x must be determined by slenderness ratio λ_{0x}. Slenderness ratio have to be determined before calculate the TCFST composite columns in theory. Mono columns are connected by perforated connecting plates and its shear stiffness is weak, so not only the influence of bending deformation but also the influence of batten plate shear deformation should be considered when TCFST composite columns bending under eccentric pressure. Therefore, it is necessary to replace the slenderness ratio with the equivalent slenderness ratio.

4.2.1 Simplified calculation model

Fig. 16 shows the stress contour of connecting plate. According to the analysis of the finite element stress contour and the failure mode of the test connecting plate, it is found that the stress is evenly distributed along the horizontal direction between the two holes of the connecting plate and there is the phenomenon of stress concentration around openings. when considering the shear

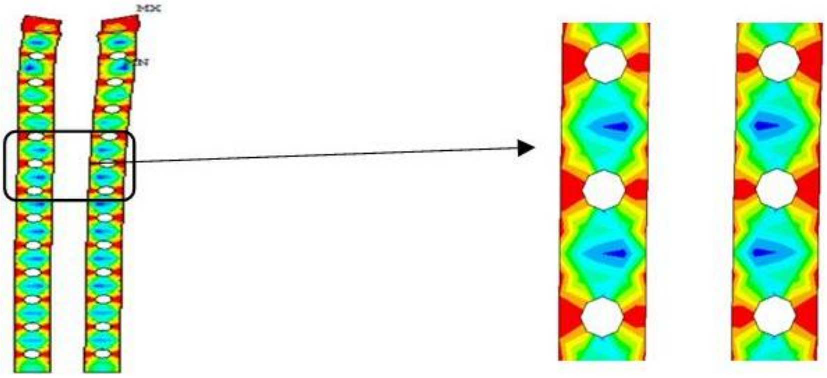

Fig. 16 Stress contour of connecting plate

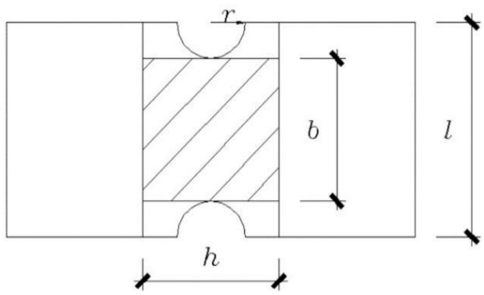

Fig. 17 Simplified model of connecting plate

deformation, it is considered that the shearing force of the mono columns is mainly transmitted through the transverse batten plate between the two holes of the connecting plate. Therefore, in this paper, when the calculation method of equivalent slenderness ratio is derived, the theoretical model is simplified to transverse batten plate model. As shown in Fig. 17.

4.2.2 Slenderness ratio formula

According to the theory of elastic stability (Leonard and George 2005, Chen *et al*. 2009), equivalent slenderness ratio formula can be deduced

$$\lambda_0 = \sqrt{\lambda^2 + \pi^2 \gamma_1 \sum_{i=1}^{n} (E_s A_{si} + E_c A_{ci})} = \sqrt{\lambda^2 + \pi^2 \gamma_1 \sum_{i=1}^{n} E_s A_{0i}} \tag{2}$$

Where, λ_0 is equivalent slenderness ratio of the TCFST column; λ_0 is the original slenderness ratio; γ_1 is the unit shear angle as explained later Eq. (7); n is the number of square steel tubular columns; E_s is the elastic modulus of steel; A_{si} is the cross-sectional area of single square steel tube; E_c is the elastic modulus of concrete; A_{ci} is the cross-sectional area of filled-concrete of single square steel tube, $A_{0i} = A_{si} + \frac{E_c}{E_s} A_{si}$ is the conversion area of single Concrete-filled Square Steel Tubular Columns.

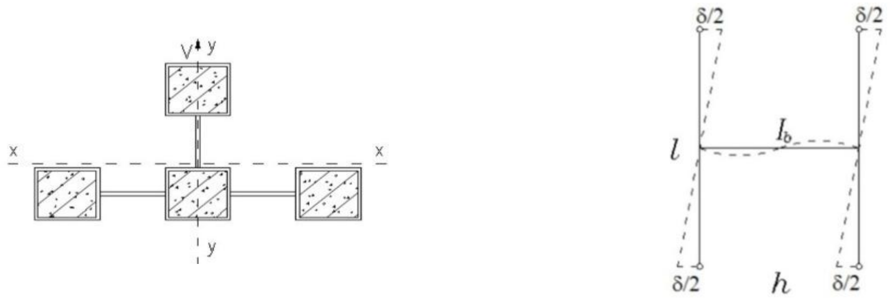

Fig. 18 Calculation diagram of batten plate model

4.2.3 The slenderness ratio calculation of bending buckling around asymmetrical axis (X-X axis)

Shear stiffness calculation

As shown in Fig. 18. When batten plate model work under shear force *V*. Then, the moment at both ends of the batten plate is *Vl* / 2.

Angular displacement at batten plate both ends

$$\theta = \frac{Vlh}{12E_sI_b} \tag{3}$$

The transverse displacement caused by the bending deformation of batten plate

$$\delta_1 = \frac{\theta l}{2} = \frac{Vhl}{24E_sI_b} \tag{4}$$

The column limb stiffness is far larger than the stiffness of batten plate, so the lateral displacement caused by column limb bending deformation can be ignored. Then the shear strain of column element along Y-axis

$$\varepsilon = \frac{\delta_1}{0.5l} = \frac{Vhl}{12E_sI_b} \tag{5}$$

The shear stiffness of the batten plate along Y-axis direction

$$K = \frac{V}{\varepsilon} = \frac{12E_sI_s}{hl} \tag{6}$$

Where, h is the width of perforated connecting plate; l is openings spacing; E_s is elastic modulus of steel. I_b is the batten plate sectional moment of inertia. I_S is the composite column sectional moment of inertia.

Equivalent slenderness ratio

The unit shear angle is

$$\gamma_1 = \frac{V_1}{K} = \frac{hl}{12E_sI_b} \tag{7}$$

Then, the slenderness ratio calculation of bending buckling is

$$\pi^2\gamma_1\sum_{i=1}^{n}E_sA_{0i}=\frac{4\pi^2hlE_sA_{0i}}{12E_sI_b}=\frac{\pi^2hlA_{0i}}{3I_b}=\frac{\pi^2hl}{3}\frac{A_{0i}}{A_b}\frac{A_b}{I_b} \tag{8}$$

$$\lambda_{0x}=\sqrt{\lambda_x^2+\frac{\pi^2hl}{3}\frac{A_{0i}}{A_b}\frac{A_b}{I_b}}=\sqrt{\lambda_x^2+\frac{\pi^2hl}{3}\frac{1}{\varphi_b}\frac{1}{i_b^2}} \tag{9}$$

Where, $i_b=\sqrt{\frac{I_b}{A_b}}$ is turning radius of single lacing bar, $\varphi_b=\frac{A_b}{A_{0i}}$, $A_{0i}=A_{si}+\frac{E_c}{E_s}A_{ci}$ is the conversion area of single Concrete-filled Square Steel Tubular Columns.

4.3 Parametric finite element analysis

The feasibility of the finite element method has been verified in the third chapter. In order to verify the applicability of the theoretical formula, parametric FEM analysis has been undertaken. In this study, factors that were taken into discussion including thickness of tube flange and connecting plate thickness. Key factors of different models were marked in Table 6.

The load-displacement curves obtained by the parametric FEM analysis as shown in Fig. 19. The failure load p_u^f obtained from the load-displacement curves are listed in Table 7 and they are compared with the experimental ones p_u^e and the ultimate bearing capacity P_u calculatted by Eq. (1). It can be seen that the majority of the error between theoretical calculation results and the ultimate bearing capacity predicted by the finite element is less than 10%. It shows that the theoretical calculation method of the bearing capacity is advisable.

Table 6 List of analytical specimens

Specimens	Tube flange (t_c)/mm	Connecting plate (t_b)/mm
GZ1(GZ1-4-6)	4	6
GZ1-6-6	6	6
GZ1-8-6	8	6
GZ1-4-3	4	3
GZ1-4-10	4	10
GZ2(GZ2-4-6)	4	6
GZ2-6-6	6	6
GZ2-8-6	8	6
GZ2-4-3	4	3
GZ2-4-10	4	10
GZ3(GZ3-4-6)	4	6
GZ3-6-6	6	6
GZ3-8-6	8	6
GZ3-4-3	4	3
GZ3-4-10	4	10

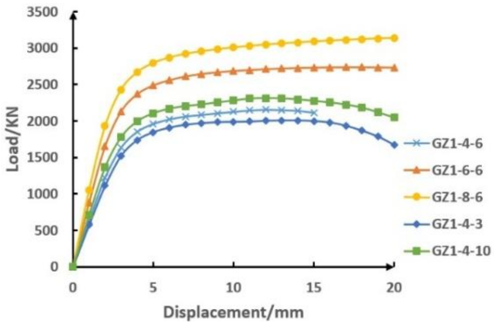

(a) GZ1 series

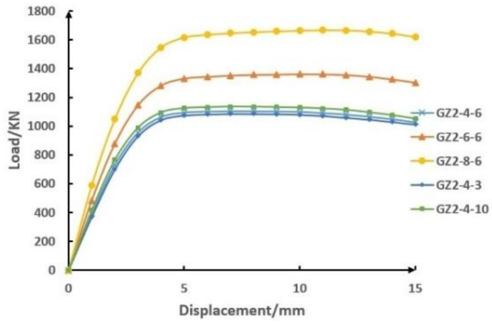

(b) GZ2 series

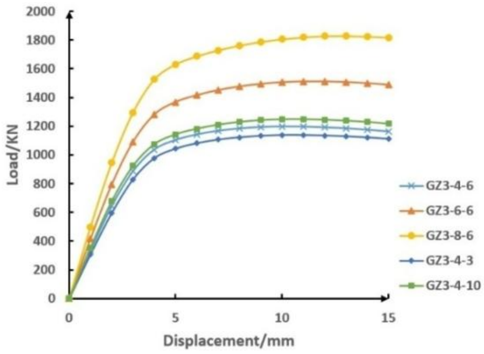

(c) GZ3 series

Fig. 19 Load-displacement curves

Table 7 Comparison of bearing capacity

Specimens	Ultimate bearing capacity				
	p_u^e (kN)	p_u^f (kN)	P_u (kN)	p_u/p_u^f	P_u/p_u^e
GZ1(GZ1-4-6)	2233	2165	2421	1.118	1.084
GZ1-6-6	--	2738	2916	1.065	--
GZ1-8-6	1301	3213	3438	1.070	--
GZ1-4-3	--	2018	2170	1.075	--
GZ1-4-10	--	2314	2573	1.111	--
GZ2(GZ2-4-6)	1211	1105	1095	0.991	0.904
GZ2-6-6	--	1362	1122	0.824	--
GZ2-8-6	--	1659	1345	0.811	--
GZ2-4-3	--	1084	979	0.903	--
GZ2-4-10	--	1135	1046	0.922	--
GZ3(GZ3-4-6)	1301	1196	1152	0.962	0.887
GZ3-6-6	--	1510	1362	0.902	--
GZ3-8-6	--	1827	1543	0.845	--
GZ3-4-3	--	1138	1110	0.975	--
GZ3-4-10	--	1248	1203	0.964	--

5. Conclusions

In this paper, Three TCFST composite columns were tested under eccentric compression and fifteen finite element specimens were conducted parametric analysis. According to results of experiments and finite element analysis, an analytical method for calculation of the eccentric compression bearing capacity of TCFST composite columns was proposed. The main conclusions can be drawn as follows:

- Three experimental results show that failure mode of the eccentric compression columns is flexural instability of the whole specimen, mono column performs flexural buckling. Specimens show good ductility and load-bearing capacity. All specimens were destroyed, mainly caused by the yield of the loading mono column.
- The analysis results of finite element including the failure mode, the load displacement curve and the ultimate load-bearing capacity are in a good agreement with the test results. Feasibility of finite element analysis is proved.
- According to the analysis of the finite element stress contour and the test failure mode of the connecting plate, it is found that the stress is evenly distributed along the horizontal direction between the two holes of the connecting plate.
- Results of theoretical calculation, parametric FEM analysis and eccentric compression experiment accord well with each other. It shows that the theoretical calculation method of the bearing capacity is advisable.

Acknowledgments

The research described in this paper was financially supported by the National Natural Science Foundations of China (No. 51268054 and No. 51468061) and the Natural Science Foundation of Tianjin City, China (No. 13JCQNJC07300). The financial supports are greatly appreciated.

References

Chen, Z.H., Rong, B. and Apostolos, F. (2009), "Axial compression stability of a crisscross section column composed of concrete-filled square steel tubes", *J. Mech. Mater. Struct.*, **4**(10), 1787-1799.

Chen, Z., Xu, J. and Xue, J. (2015), "Hysteretic behavior of special shaped columns composed of steel and reinforced concrete (SRC)", *Earthq. Eng. Eng. Vib.*, **14**(2), 329-345.

Chen, Z., Xu, J., Chen, Y. and Xue, J. (2016), "Axial compression ratio limit values for steel reinforced concrete (SRC) special shaped columns", *Steel Compos. Struct., Int. J.*, **20**(2), 295-316.

Dundar, C. and Tokgoz, S. (2012), "Strength of biaxially loaded high strength reinforced concrete columns", *Struct. Eng. Mech., Int. J.*, **44**(5), 649-661.

Dundar, C., Tokgoz, S., Tanrikulu, A.K. and Baran, T. (2008), "Behaviour of reinforced and concrete-encased composite columns subjected to biaxial bending and axial load", *Build. Environ.*, **43**(6), 1109-1120.

Fang, L., Zhang, B., Jin, G.F., Li, K.W. and Wang, Z.L. (2015), "Seismic behavior of concrete-encased steel cross-shaped columns", *J. Construct. Steel Res.*, **109**, 24-33.

Leonard, S. and George, F. (2005), *Applied Structural Steel Design*, Tsinghua University Press, Beijing, China.

Ren, Q.X., Han, L.H., Lam, D. and Chao, H. (2014), "Experiments on special-shaped CFST stub columns under axial compression", *J. Construct. Steel Res.*, **98**, 123-133.

Rong, B., Chen, Z., Apostolos, F. and Yang, N. (2012), "Axial Compression Behavior and Analytical Method of L-Shaped Column Composed of Concrete-Filled Square Steel Tubes", *Transact. Tianjin Univ.*, **18**, 180-187.

Shen, Z.Y., Lei, M., Li, Y.Q., Lin, Z.Y. and Luo, J.H. (2013), "Experimental study on seismic behavior of concrete-filled L-shaped steel tube columns", *Adv. Struct. Eng.*, **16**(7), 1235-1247.

Tu, Y.Q., Shen, Y.F. and Li, P. (2014), "Behaviour of multi-cell composite T-shaped concrete-filled steel tubular columns under axial compression", *Thin-Wall. Struct.*, **85**, 57-70.

Yang, Y.F. and Han, L.H. (2011), "Behavior of concrete-filled steel tubular (CFST) stub columns under eccentric partial compression", *Thin-Wall. Struct.*, **49**(2), 379-395.

Yang, Y., Yang, H. and Zhang, S. (2010), "Compressive behavior of T-shaped concrete filled steel tubular columns", *Int. J. Steel Struct.*, **10**(4), 419-430.

Tokgoz, S. and Dundar, C. (2008), "Experimental tests on biaxially loaded concrete-encased composite columns", *Steel Compos. Struct., Int. J.*, **8**(5), 423-438.

Zhou, T., Chen, Z. and Liu, H. (2012), "Seismic behavior of special shaped column composed of concrete filled steel tubes", *J. Construct. Steel Res.*, **75**(4), 131-141.

Zhou, T., Xu, M., Wang, X., Chen, Z. and Qin, Y. (2015), "Experimental study and parameter analysis of L-shaped composite column under axial loading", *Int. J. Steel Struct.*, **15**(4),797-807.

Zuo, Z.L., Cai, J., Yang, C. and Chen, Q.J. (2012), "Eccentric load behavior of L-shaped CFT stub columns with binding bars", *J. Construct. Steel Res.*, **72**, 88-98.

CC